Non-axisymmetric buckling of elastic-plastic annular plates

Ülo Lepik

Institute of Applied Mathematics, University of Tartu, Vanemuise 46, 51014 Tartu, Estonia; ylepik@ut.ee

Abstract. The elastic-plastic stability of an annular plate under uniform radial loads applied at its edges is considered. Emphasis is laid on the non-axisymmetric buckling forms since the assumption of symmetric buckling does not necessarily lead to the lowest critical load. As a constitutive law elastic-plastic relations with linear strain hardening and the Tresca yield condition are adopted. The buckling equation is integrated by the Runge–Kutta method. Numerical results for three types of loading and two versions of the boundary conditions are presented.

Key words: annular plates, non-axisymmetric buckling, elastic-plastic material, Tresca yield condition.

1. INTRODUCTION

Elastic stability of circular and annular plates has been treated by several researchers under various loading and boundary conditions. In most of these papers the buckling forms are assumed to be axisymmetric. In many cases non-axisymmetric buckling forms also exist and the assumption of axisymmetric buckling may overestimate the stability of the plate. In the case of non-axisymmetric buckling we have to choose such a number of waves which leads to the lowest critical load.

Non-axisymmetric buckling of elastic annular plates was discussed by Yamaki [1], who considered a uniformly compressed annulus for 12 different versions of the boundary conditions. The solution is given via elliptic functions. Mansfield [2] considered an elastic plate subjected to a uniform radial load along the inner circle. It is assumed that the stresses decay inversely as the square of the distance from the

centre of the circle. It is shown that if the radial stress is compressive, the buckling mode will have rotational symmetry, but if the radial stress is tensile, the plate buckles into a number of circumferential waves (the hoop stresses are compressive). Radwańska and Waszczyszyn [3] examined the postbuckling behaviour of annular plates. The problem is solved with the aid of the orthogonalization method. Numerical examples are given for the free inner edge and for the clamped external edge; compressive load is applied to the outer edge. In the paper by Kumelj and Kosel [4], stability of annular plates made of rectilinearly orthotropic material is discussed. Noteworthy is also the paper by Kosel and Chen Jin [5] dealing with the buckling of an annular plate subjected to two opposite locally acting pressures and supported at two points. To increase the buckling strength of the plate, additional radial or circular supports can be used. The effect of a circular rigid support was examined by Laura et al. [6] and Lepik [7]. Thermal stability of annular elastic-plastic plates with application to brake discs is discussed by Fan and Lippmann [8].

In this paper elastic-plastic buckling of annular plates under uniform radial loads applied at its edges is analysed. In Section 2 the problem statement is presented. The prebuckling state is investigated in Section 3. In Sections 4 and 5 the buckling equations are put together. Numerical calculations for six versions of loading and boundary conditions, for which non-axisymmetric buckling might be expected, are given in Section 6. These results are discussed in Section 7. In the final Section 8 some conclusions are drawn.

2. PROBLEM STATEMENT

Let us consider a thin annular plate under uniform forces applied at its edge and acting in the midplane of the plate. These forces invoke a stress state, which is characterized by radial stress $\sigma_r^*(r^*)$ and by circumferential stress $\sigma_\theta^*(r^*)$, where r^* is the radial coordinate. We shall denote the radius of the inner edge by a and the radius of the outer edge by b; h is the thickness of the plate.

The equation of equilibrium is

$$\frac{d\sigma_r^*}{dr^*} + \frac{\sigma_r^* - \sigma_\theta^*}{r^*} = 0. \tag{1}$$

With the purpose of simplifying subsequent expressions, the following notations are introduced:

$$r = \frac{r^*}{b}, \quad \gamma = \frac{a}{b}, \quad \sigma_r = \frac{\sigma_r^*}{\sigma_s}, \quad \sigma_\theta = \frac{\sigma_\theta^*}{\sigma_s}, \quad p = \frac{P^*}{\sigma_s h}. \tag{2}$$

Here P^* is strength of the external force, σ_s stands for the yield stress of the material.

Equation (1) takes the form

$$r\sigma_r' + \sigma_r - \sigma_\theta = 0, \tag{3}$$

where the prime denotes differentiation with respect to the nondimensional radius r. In nondimensional form $r = \gamma$ and $r = 1$ represent the inner and outer edges, respectively.

Below, the following three loading types are considered.

Case A: Along the outer edge a uniform compressive stress is applied so that the boundary conditions are $\sigma_r(1) = -p, \ \sigma_r(\gamma) = 0$.

Case B: Along the inner edge a uniform tensile stress acts; in this case we have $\sigma_r(1) = 0, \ \sigma_r(\gamma) = p$.

Case C: Uniformly distributed compressive stresses act along the edges and we get the boundary conditions $\sigma_r(1) = \sigma_r(\gamma) = -p$.

The integrals of Eq. (3) are well known in the case of elastic deformations (see, e.g., Timoshenko [9]); therefore here only the final results are presented.

Case A:

$$\sigma_r = -\frac{p}{1-\gamma^2}\left(1 - \frac{\gamma^2}{r^2}\right), \quad \sigma_\theta = -\frac{p}{1-\gamma^2}\left(1 + \frac{\gamma^2}{r^2}\right); \qquad (4)$$

Case B:

$$\sigma_r = \frac{\gamma^2 p}{1-\gamma^2}\left(\frac{1}{r^2} - 1\right), \quad \sigma_\theta = -\frac{\gamma^2 p}{1-\gamma^2}\left(1 + \frac{1}{r^2}\right); \qquad (5)$$

Case C:

$$\sigma_r = \sigma_\theta = -p = \text{const.} \qquad (6)$$

It follows from (4)–(6) that $\sigma_\theta < 0$ and $|\sigma_r| < \sigma_\theta$ for $r \in [\gamma, 1]$. This circumstance creates favourable conditions for non-axisymmetric buckling.

3. PREBUCKLING STRESS STATE

It is considerably more difficult to integrate Eq. (3) in the plastic case than in the elastic case. To illustrate this assertion, let us turn to the monograph by Il'yushin [10]. Making use of the deformation theory and the von Mises yield condition, he solved Eq. (3) for $e_{zz} = 0, \ \sigma_{zz} \neq 0$ (plane strain); his solution takes about ten pages. In our paper a plane stress problem $e_{zz} \neq 0, \ \sigma_{zz} = 0$ must be solved; hereby the solution is still more complicated. Evidently we must seek for some simplifications.

One possibility is to replace the von Mises yield condition with the Tresca condition. For this purpose we introduce the quantity

$$Q = \max\left(|\sigma_r|, |\sigma_\theta|, |\sigma_r - \sigma_\theta|\right). \qquad (7)$$

If $Q < 1$, the deformation is elastic, for $Q \geq 1$ we get the elastic-plastic case. This yield condition is shown in Fig. 1.
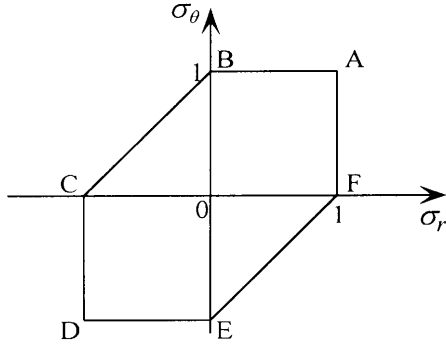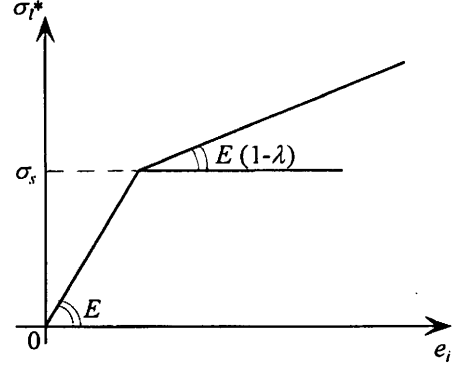
Fig. 1. Tresca yield condition.

Fig. 2. Stress-strain diagram with linear strain hardening.

For further simplification we assume that the material is linearly strain-hardening (Fig. 2). If σ_i^* and e_i are effective stress and effective strain, then according to the diagram in Fig. 2 we find

$$\sigma_i^* = \sigma_s + E(1 - \lambda)(e_i - e_s). \tag{8}$$

Introducing the symbol $\sigma_i = \sigma_i^*/\sigma_s$, we can rewrite Eq. (8) in the non-dimensional form

$$\sigma_i = \lambda + (1 - \lambda)\frac{e_i}{e_s}. \tag{9}$$

Here $\lambda = \mathrm{const}$ is the strain-hardening parameter. The inequalities $0 \leq \lambda \leq 1$ hold; limit cases correspond to the elastic and ideal-plastic material, respectively.

In the following treatment Cases A, B, and C must be considered separately.

Case A. Making use of (4) and (7), we find $Q = -\sigma_\theta$. Consequently, transition into the plastic state takes place through the segment DE in Fig. 1. It follows from the associated flow rule that

$$de_r^p = 0, \quad de_\theta^p = \frac{1}{H'}d\sigma_\theta^*. \tag{10}$$

Here e_r^p and e_θ^p are plastic parts of the strains. The quantity H' is defined as $H' = d\sigma_i^*/de_i^p$, where e_i^p is the effective plastic strain. In the case of the linear strain-hardening material it follows from (8) that

$$H' = E\frac{1 - \lambda}{\lambda}. \tag{11}$$

Next we integrate Eqs. (10) and present the result in nondimensional form

$$e_r^p = 0, \quad e_\theta^p = \frac{e_s \lambda}{1 - \lambda}(\sigma_\theta + 1). \tag{12}$$

It is assumed that the strains are divisible into elastic and plastic parts

$$e_r = e_r^e + e_r^p, \quad e_\theta = e_\theta^e + e_\theta^p. \tag{13}$$

The elastic parts are (ν is the Poisson ratio)

$$e_r^e = e_s(\sigma_r - \nu\sigma_\theta), \quad e_\theta^e = e_s(\sigma_\theta - \nu\sigma_r). \tag{14}$$

Making use of (12)–(14), we find

$$\sigma_r = A \left\{ \frac{1}{e_s} \left[e_r + \nu(1 - \lambda)e_\theta \right] - \nu\lambda \right\},$$

$$\sigma_\theta = A \left[\frac{1}{e_s} \left(e_r \nu + e_\theta \right)(1 - \lambda) - \lambda \right], \tag{15}$$

where $A = (1 - \nu^2 + \lambda\nu^2)^{-1}$.

Denoting the nondimensional radial displacement by $u = u^*/b$, we have

$$e_r = u', \quad e_\theta = u/r. \tag{16}$$

Replacing (15) and (16) into Eq. (3), we find

$$r^2 u'' + r u' - (1 - \lambda)u = -e_s\lambda(1 - \nu)r. \tag{17}$$

The general solution of this equation is

$$u = C_1^p r^\Lambda + C_2^p r^{-\Lambda} - e_s(1 - \nu)r, \quad (\Lambda = \sqrt{1 - \lambda}). \tag{18}$$

Here C_1^p, C_2^p are the integration constants. Taking into account (16) and (18), we can rewrite (15) in the form

$$\sigma_r = \alpha_1 r^{\Lambda-1} C_1^p + \alpha_2 r^{-\Lambda-1} C_2^p - 1,$$

$$\sigma_\theta = \beta_1 r^{\Lambda-1} C_1^p + \beta_2 r^{-\Lambda-1} C_2^p - 1, \tag{19}$$

where

$$\alpha_1 = \frac{A}{e_s} \left[\Lambda + \nu(1 - \lambda) \right], \quad \alpha_2 = \frac{A}{e_s} \left[-\Lambda + \nu(1 - \lambda) \right],$$

$$\beta_1 = \frac{A}{e_s}(1 - \lambda)(1 + \nu\Lambda), \quad \beta_2 = \frac{A}{e_s}(1 - \lambda)(1 - \nu\Lambda). \tag{20}$$

Elastic deformations can be treated in a similar way. By doing this we find for the elastic region

$$
\begin{aligned}
u &= C_1^e r + C_2^e \frac{1}{r}, \\
\sigma_r &= \frac{1}{e_s}\left(\frac{C_1^e}{1-\nu} - \frac{C_2^e}{(1+\nu)r^2}\right), \\
\sigma_\theta &= \frac{1}{e_s}\left(\frac{C_1^e}{1-\nu} + \frac{C_2^e}{(1+\nu)r^2}\right).
\end{aligned}
\tag{21}
$$

In the present case plastic deformations appear in the zone $r \in [\gamma, \varrho]$; for $r \in [\varrho, 1]$ the deformations are elastic, ϱ is the radius separating these zones.

There are five unknown constants in (19)–(21): C_1^e, C_2^e, C_1^p, C_2^p, and the radius ϱ (or the corresponding load parameter p). To evaluate these constants, we shall satisfy the boundary conditions $\sigma_r(\gamma) = 0$, $\sigma_r(1) = -p$, the condition $\sigma_\theta(\varrho-) = -1$, and the continuity conditions for u and σ_r at $r = \varrho$. Doing so we get a system of five equations. To solve this system, it is expedient to prescribe ϱ and calculate p from the condition $\sigma_r(1) = -p$. The final results can be presented in the form

$$
\begin{aligned}
C_1^p &= \left(\alpha_1 \gamma^{\Lambda-1} - \frac{\alpha_2 \beta_1}{\beta_2}\varrho^{2\Lambda}\gamma^{-\Lambda-1}\right)^{-1}, \\
C_2^p &= -\frac{\beta_1}{\beta_2}\varrho^{2\Lambda}C_1^p, \\
C_1^e &= \frac{1}{2}(1-\nu)\left[e_s(1+\nu)\sigma_r(\varrho-) + \frac{1}{\varrho}u(\varrho-)\right], \\
C_2^e &= \varrho[u(\varrho-) - C_1^e\varrho], \\
p &= \frac{1}{e_s}\left(-\frac{C_1^e}{1-\nu} + \frac{C_2^e}{1+\nu}\right),
\end{aligned}
\tag{22}
$$

where $\sigma_r(\varrho-)$ and $u(\varrho-)$ are evaluated from (18) and (19)$_1$.

As an example the calculations were carried out for: (i) $\gamma = 0.2$, $p = 0.4$ (Fig. 3a, elastic case) and (ii) $\gamma = 0.2$, $p = 0.78$, $\varrho = 0.6$ (Fig. 3b, elastic-plastic case).

Case B. It follows from (5) that

$$
Q = \sigma_r - \sigma_\theta.
$$

Consequently, plastic deformations appear if we move through the edge EF in Fig. 1.

According to the associated flow rule, we have

$$
de_r^p = \frac{1}{H'}(d\sigma_r^* - d\sigma_\theta^*), \quad de_\theta^p = \frac{1}{H'}(d\sigma_\theta^* - d\sigma_r^*).
$$

The integral form of these equations, if we take into account (11), is

$$e_r^p = \frac{\lambda e_s}{1 - \lambda}(\sigma_r - \sigma_\theta - 1), \quad e_\theta^p = -\frac{\lambda e_s}{1 - \lambda}(\sigma_r - \sigma_\theta - 1). \tag{23}$$

For the elastic parts of the strains e_r^e and e_θ^e, (14) holds. Making use of (13), we find

$$
\begin{aligned}
\sigma_r &= \frac{1}{(1 - \nu)(1 + K)}\left[\frac{1}{e_s}(e_r + Ke_\theta) + \lambda(1 - \nu)\right], \\
\sigma_\theta &= \frac{1}{(1 - \nu)(1 + K)}\left[\frac{1}{e_s}(Ke_r + e_\theta) - \lambda(1 - \nu)\right],
\end{aligned}
\tag{24}
$$

where $K = \nu + \lambda(1 - \nu)$.
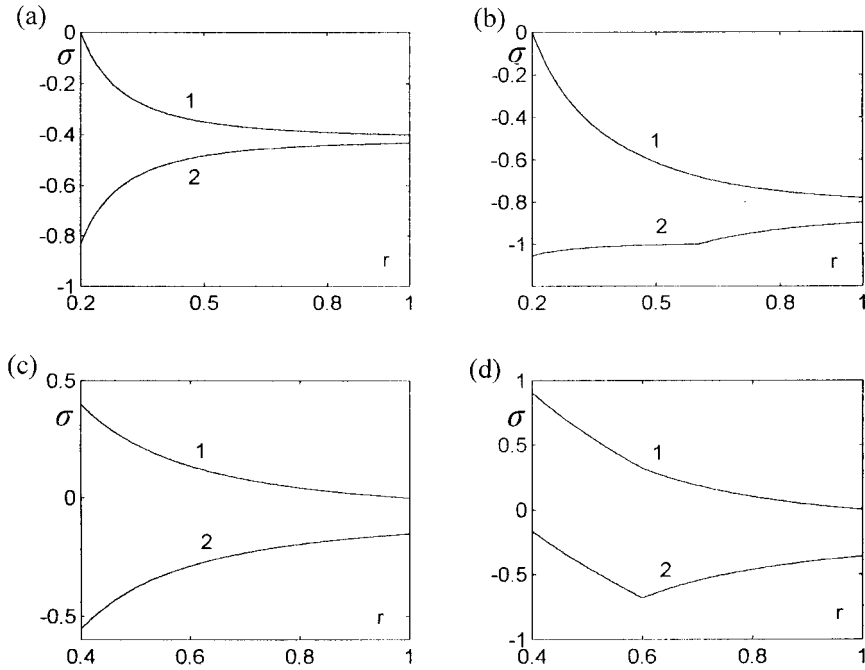

Fig. 3. Stresses versus radial coordinate: 1, radial stress σ_r; 2, hoop stress σ_θ. The following versions are considered: (a) Case A, $p = 0.4$, $\gamma = 0.2$ (elastic); (b) Case A, $p = 0.78$, $\varrho = 0.6$, $\gamma = 0.2$ (elastic-plastic); (c) Case B, $p = 0.4$, $\gamma = 0.4$ (elastic); (d) Case B, $p = 0.91$, $\varrho = 0.6$, $\gamma = 0.4$ (elastic-plastic).

The following way of solution is quite similar to that used in Case A. Therefore we leave out the details and confine us to the final results.

In the plastic zone $r \in [0, \varrho]$ we have

$$u = C_1^p r + C_2^p \frac{1}{r} - \lambda e_s r (\ln r - 0.5),$$

$$e_s \sigma_r = \frac{1}{1-\nu} C_1^p - \frac{1-\lambda}{K+1} \frac{1}{r^2} C_2^p - \frac{\lambda e_s \ln r}{1-\nu} + \frac{\lambda e_s (1+\lambda)}{2(K+1)}, \qquad (25)$$

$$e_s \sigma_\theta = \frac{1}{1-\nu} C_1^p + \frac{1-\lambda}{K+1} \frac{1}{r^2} C_2^p - \frac{\lambda e_s \ln r}{1-\nu} - \frac{\lambda e_s (1+\lambda)}{2(K+1)}.$$

These results are applicable also in the elastic zone $r \in [\varrho, 1]$ if we replace $\lambda \to 0$, $C_1^p \to C_1^e$, $C_2^p \to C_2^e$. Satisfying the conditions

$$\sigma_r(\gamma) = p, \quad \sigma_r(1) = 0, \quad \sigma_r(\varrho+) - \sigma_\theta(\varrho+) = 1,$$

$$\sigma_r(\varrho+) = \sigma_r(\varrho-), \quad u(\varrho+) = u(\varrho-),$$

we find

$$C_1^e = -\frac{1}{2} e_s \varrho^2 (1-\nu), \quad C_2^e = -\frac{1}{2} e_s \varrho^2 (1+\nu),$$

$$C_1^p = -\lambda e_s \ln \varrho - \frac{1}{2} e_s \varrho^2 (1-\nu), \qquad (26)$$

$$C_2^p = -\frac{1}{2} e_s \varrho^2 (1+\nu-\lambda), \quad p = \sigma_2(\gamma).$$

Numerical calculations for $\gamma = 0.4$, $p = 0.4$ (elastic case) and for $\gamma = 0.4$, $\varrho = 0.6$, $p = 0.91$ (elastic-plastic case) are shown in Fig. 3c,d.

Case C. Equations (6) hold also in the elastic-plastic case $p > 1$ (now the whole plate is in the plastic state).

It is useful to know the load p_+, at which first plastic deformations appear. This load can be determined from the condition $\sigma_\theta(\gamma) = -1$ (Case A) or $\sigma_r(\gamma) - \sigma_\theta(\gamma) = 1$ (Case B). Taking into account (4) and (5), we see that in both cases

$$p_+ = 0.5(1 - \gamma^2). \qquad (27)$$

In Case C, $p_+ = 1$.

4. VARIATION OF STRAINS AND STRESSES

To derive the bifurcation equation, we must vary the strain and stress state. The strain variations for a point off the middle surface at distance z^* are (see, e.g., [11], p. 156):

$$\delta e_r = \delta\varepsilon_r - z^*\frac{\partial^2 w^*}{\partial r^{*2}},$$

$$\delta e_\theta = \delta\varepsilon_\theta - z^*\left(\frac{1}{r^*}\frac{\partial w^*}{\partial r^*} - \frac{1}{r^{*2}}\frac{\partial^2 w^*}{\partial\theta^2}\right), \qquad (28)$$

$$\delta e_{r\theta} = \delta\varepsilon_{r\theta} - 2z^*\left(\frac{1}{r^*\partial\theta}\frac{\partial w^*}{\partial r^*} - \frac{1}{r^2}\frac{\partial^2 w^*}{\partial\theta}\right).$$

Here ε_r, ε_θ, $\varepsilon_{r\theta}$ denote the middle surface strains, w^* is the deflection of the buckled plate, θ is the polar angle. Next we introduce nondimensional quantities $w = w^*/h$, $z = z^*/h$ and seek nondimensional deflections in the form

$$w(r,\theta) = W(r)\cos m\theta \quad (m = 0, 1, 2, 3, ...). \qquad (29)$$

In view of (28), we find

$$\delta e_r = \delta\varepsilon_r - \left(\frac{h}{b}\right)^2 zW''\cos m\theta,$$

$$\delta e_\theta = \delta\varepsilon_\theta - \left(\frac{h}{b}\right)^2 z\left(\frac{1}{r}W' + \frac{m^2}{r^2}W\right)\cos m\theta, \qquad (30)$$

$$\delta e_{r\theta} = \delta\varepsilon_{r\theta} + 2m\left(\frac{h}{b}\right)^2 z\left(\frac{1}{r}W' - \frac{1}{r^2}W\right)\sin m\theta.$$

To calculate the stress variations $\delta\sigma_x$, $\delta\sigma_\theta$, we must consider Cases A, B, and C separately.

Case A. By varying Eqs. (15) we find

$$e_s\delta\sigma_r = s_1\delta e_r + s_2\delta e_\theta,$$

$$e_s\delta\sigma_\theta = s_3\delta e_r + s_4\delta e_\theta, \qquad (31)$$

where

$$s_1 = A, \quad s_2 = A\nu(1-\lambda), \quad s_3 = s_2, \quad s_4 = A(1-\lambda). \qquad (32)$$

Case B. Here we vary (24). Equations (31) hold if we take

$$s_1 = \frac{1}{(1-\nu)(1+K)}, \quad s_2 = \frac{K}{(1-\nu)(1+K)}, \quad s_3 = s_2, \quad s_4 = s_1. \qquad (33)$$

Case C. In this case $\sigma_r = \sigma_\theta = -p$ and we find ourselves in the corner D in Fig. 1. Since here plastic flow is nonunique, a special treatment is necessary. We proceed from Eqs. (19) of the paper [12], which for our case can be put into the form (31), where

$$s_1 = s_4 = \frac{4-3\lambda}{N}, \quad s_2 = s_3 = \frac{4\nu(1-\lambda)-\lambda}{N} \qquad (34)$$

94

and

$$N = 2(1 + \nu)[2(1 - \lambda)(1 - \nu) + \lambda].$$

Equations (32)–(34) are valid also in the elastic case if we take $\lambda = 0$.

5. BUCKLING EQUATION

To analyse the bifurcation process, we shall start from the equilibrium equations (see, e.g., (2.162)–(2.165) in the text-book [11]). For our problem and in our notations these equations obtain the form

$$rQ_r = M_r - M_\theta + r\frac{\partial M_r}{\partial r} + \frac{\partial M_{r\theta}}{\partial \theta},$$

$$rQ_\theta = \frac{\partial M_\theta}{\partial \theta} + 2M_{r\theta} + r\frac{\partial M_{r\theta}}{\partial r},$$

$$r\left(\sigma_r\frac{\partial^2 w}{\partial r^2} + \frac{\partial \sigma_r}{\partial r}\frac{\partial w}{\partial r}\right) + \sigma_r\frac{\partial w}{\partial r} + \frac{1}{r}\left(\sigma_\theta\frac{\partial^2 w}{\partial \theta^2} + \frac{\partial \sigma_\theta}{\partial \theta}\frac{\partial w}{\partial \theta}\right)$$

$$+ Q_r + r\frac{\partial Q_r}{\partial r} + \frac{\partial Q_\theta}{\partial \theta} = 0. \tag{35}$$

Here M_r, M_θ, $M_{r\theta}$ are nondimensional moments, which can be calculated from the formulae

$$M_r = 4\int_{-0.5}^{0.5}\delta\sigma_r z dz, \quad M_\theta = 4\int_{-0.5}^{0.5}\delta\sigma_\theta z dz, \quad M_{r\theta} = 4\int_{-0.5}^{0.5}\delta\sigma_{r\theta} z dz, \tag{36}$$

and Q_r, Q_θ are nondimensional transverse shear forces.

In the bifurcation theory of elastic-plastic structures a complicated problem is to determine the size and form of the elastic unloading zone. Several discussions have been held about this problem, nevertheless we do not yet have a mathematically correct solution. Therefore we make use of the Shanley concept, according to which unloading at the bifurcation point may be neglected. Such a simplified approach is favoured by the following facts:

(i) The Shanley concept has been successfully applied by many authors; the results obtained are in good accordance with experimental data.

(ii) By neglecting the strain reversal we obtain the lower bound for the critical loads.

Further discussion about the admissibility and expediency of the Shanley concept can be found in [13,14].

Since according to the Shanley concept no unloading takes place, we can integrate (36). Taking into account (29)–(31), we find

$$
\begin{aligned}
M_r &= -\frac{\mu}{3}\cos m\theta \left[s_1 W'' + s_2 \left(\frac{1}{r}W' - \frac{m^2}{r^2}W \right) \right], \\
M_\theta &= -\frac{\mu}{3}\cos m\theta \left[s_3 W'' + s_4 \left(\frac{1}{r}W' - \frac{m^2}{r^2}W \right) \right],
\end{aligned}
\tag{37}
$$

where $\mu = (h/b)^2/e_s$.

Now let us evaluate $M_{r\theta}$. Since before bifurcation $\sigma_{r\theta} = 0$, it is logical to assume that the variation of the shear stress $\delta\sigma_{r\theta}$ is elastic and can be calculated according to the formula

$$
\delta\sigma_{r\theta} = \frac{G}{\sigma_s}\delta e_{r\theta} = \frac{\delta e_{r\theta}}{2(1+\nu)e_s},
\tag{38}
$$

where G is the shear modulus. It follows from (36) that

$$
M_{r\theta} = \frac{1}{3}\frac{\mu m}{1+\nu}\sin m\theta \left(\frac{1}{r}W' - \frac{1}{r^2}W \right).
\tag{39}
$$

Next we calculate Q_r, Q_θ from $(35)_1$ and $(35)_2$ and replace the results into $(35)_3$. By doing this we find

$$
W'''' + A_3 W''' + A_2 W'' + A_1 W' + A_0 W = 0,
\tag{40}
$$

where

$$
\begin{aligned}
A_3 &= (2s_1 + s_2 - s_3)\frac{1}{s_1 r}, \\
A_2 &= -\left[s_4 + m^2 \left(s_2 + s_3 + \frac{2}{1+\nu} \right) \right]\frac{1}{s_1 r^2} - \frac{12\sigma_r}{s_1 \mu}, \\
A_1 &= \left[s_4 + 2m^2 \left(s_2 + \frac{1}{1+\nu} \right) \right]\frac{1}{s_1 r^3} - \frac{12\sigma_\theta}{s_1 \mu r}, \\
A_0 &= -m^2 \left(2s_2 + 2s_4 - m^2 s_4 + \frac{2}{1+\nu} \right)\frac{1}{s_1 r^4} + \frac{12m^2 \sigma_\theta}{s_1 \mu r^2}.
\end{aligned}
\tag{41}
$$

In the elastic region, where $r > \varrho$, we take again $\lambda = 0$.

To integrate (40), we must specify the boundary conditions. The main versions for this are:

(i) clamped edge $W = W' = 0$;

(ii) simply supported edge $W = M_r = 0$;

(iii) free edge $M_r = 0$ and $Q_r^* + \sigma_r^*(dw^*/dr^*) = 0$ (in dimensionless form the last equation is $Q_r + 4pW' \cos m\theta = 0$).

96

Since (38) is linear with regard to W, the superposition method can be used to solve the boundary value problem. To illustrate the application of this method, let us consider a plate with both ends clamped.

The general solution of (40) can be written in the form

$$W = C_1 W_1 + C_2 W_2 + C_3 W_3 + C_4 W_4, \tag{42}$$

where W_1, W_2, W_3, W_4 are particular solutions satisfying the boundary conditions

$$\begin{aligned}
W_1(\gamma) = 0, \quad & W_1'(\gamma) = 0, \quad & W_1''(\gamma) = 1, \quad & W_1'''(\gamma) = 0, \\
W_2(\gamma) = 0, \quad & W_2'(\gamma) = 0, \quad & W_2''(\gamma) = 0, \quad & W_2'''(\gamma) = 1, \\
W_3(\gamma) = 1, \quad & W_3'(\gamma) = 0, \quad & W_3''(\gamma) = 0, \quad & W_3'''(\gamma) = 0, \\
W_4(\gamma) = 0, \quad & W_4'(\gamma) = 1, \quad & W_4''(\gamma) = 0, \quad & W_4'''(\gamma) = 0.
\end{aligned}$$

The conditions $W(\gamma) = W'(\gamma) = 0$ are satisfied if $C_3 = C_4 = 0$. Fulfilling the conditions $W(1) = W'(1) = 0$, we get

$$\begin{aligned}
C_1 W_1(1) + C_2 W_2(1) = 0, \\
C_1 W_1'(1) + C_2 W_2'(1) = 0.
\end{aligned} \tag{43}$$

This system has a nontrivial solution if its determinant is zero:

$$D = W_1(1) W_2'(1) - W_2(1) W_1'(1) = 0. \tag{44}$$

We can choose one of the coefficients in (43) arbitrarily by taking, for example, $C_1 = 1$. Then $C_2 = -W_1(1)/W_2(1)$ and according to (42) we find

$$W(r) = W_1(r) - \frac{W_1(1)}{W_2(1)} W_2(r). \tag{45}$$

Other boundary value problems can be treated in a similar way.

To calculate the critical loads and the deflection shapes, the following two algorithms are proposed.

Algorithm 1. This algorithm is applicable to plastic buckling in the Cases A and B.

Step 1: Specify the values of ϱ and m.

Step 2: Making use of (19)–(21) in Case A and of (24)–(26) in Case B, calculate the stresses for the prebuckling state.

Step 3: Evaluate the coefficients A_0, A_1, A_2, A_3 according to (41).

Step 4: By integrating (40) find the partial solutions W_1, W_2.

Step 5: Calculate the determinant D in (44).

Step 6: If $D \neq 0$, change ϱ and return to Step 1 (making use of linear interpolation, we shall repeat this step until the condition $D = 0$ is fulfilled with the prescribed accuracy).

Step 7: Evaluate the critical load p_{cr}.

Step 8: Repeat this procedure for different values of m and find the value for which p_{cr} is minimal.

Step 9: Making use of (45) and (29), calculate the function $w = w(r, \theta)$.

Algorithm 2. This algorithm holds good for elastic buckling in Cases A and B and for Case C (elastic and plastic buckling). Algorithm 1 remains applicable if we carry out the following changes:

(i) In Steps 1 and 6, instead of ϱ, we shall prescribe the load p.

(ii) Steps 2 and 7 will be omitted.

6. NUMERICAL EXAMPLES

In the examples given below calculations were carried out for material parameters $\nu = 0.3$, $\lambda = 0.95$, $e_s = 0.004$. Equation (40) was integrated using the Runge–Kutta method with the step $\Delta = 0.01(1 - \gamma)$.

Two versions of boundary conditions were considered:

(i) Both ends of the plate are clamped (version $Cl + Cl$).

(ii) The inner edge is free, the outer edge clamped (version $Fr + Cl$).

It should be noted that for elastic deformations and also for Case C the number of parameters may be reduced by one if we introduce a new parameter

$$P = \frac{12p}{\mu}(1 - \nu^2). \tag{46}$$

Now the solutions do not depend upon the relation b/h.

The critical values of the parameter P are shown in Tables 1–3, where $\gamma = a/b$. The integer m is the wave number for which P is minimal. The symbol P^0 is the critical load for axisymmetric buckling. Dashes in the last columns of the tables indicate that axisymmetric buckling does not take place. It is essential to know the load at which the first plastic deformations appear; it is marked by p_+. The symbol $(b/h)_*$ marks the relation at which the load p_+ is attained.

For plastic deformations in Cases A and B the coordinate ϱ separating the elastic and plastic zones depends upon the relation b/h. Consequently, different values of b/h produce different buckling forms. Plastic deformations take place if $b/h < (b/h)_*$. Critical loads p for plastic buckling are listed in Tables 4 and 5, where for each value of γ two typical values of b/h, for which the critical load is calculated, are taken. Contour plots for the buckling forms are shown in Fig. 4.

Table 1. Case A, elastic buckling

γ	p_+	$(b/h)_*$	P	m	P^0
Both edges clamped					
0.2	0.48	51.2	55.1	2	69.8
0.4	0.42	69.1	88.2	4	141.8
0.6	0.32	102.8	147.0	8	360.7
0.8	0.16	213.7	318.0	20	1631.7
Outer edge clamped, inner edge free					
0.2	0.48	31.7	21.1	0	21.1
0.4	0.42	38.5	27.2	1	–
0.6	0.32	48.7	33.1	3	–
0.8	0.16	88.1	54.3	8	–

Table 2. Case B, elastic buckling

γ	p_+	$(b/h)_*$	P	m	P^0
Both edges clamped					
0.2	0.48	180.8	691.7	4	12819
0.4	0.42	140.3	364.0	6	12080
0.6	0.32	152.0	324.6	10	28310
0.8	0.16	253.1	454.0	22	63109
Outer edge clamped, inner edge free					
0.2	0.48	141.8	421.6	1	963
0.4	0.42	98.7	178.8	3	580
0.6	0.32	88.6	109.7	5	735
0.8	0.16	116.1	94.2	10	2020

Table 3. Case C, elastic and plastic buckling

γ	$(b/h)_*$	P_{el}	m_{el}	P_{el}^0	P_{pl}	m_{pl}	P_{pl}^0
Both edges clamped							
0.2	35.6	55.7	2	62.2	141.2	2	157.7
0.4	47.9	101.0	3	109.2	255.9	3	276.7
0.6	72.1	228.7	5	244.7	579.8	5	620.2
0.8	144.3	917.3	11	977.5	2325.8	11	2477.3
Outer edge clamped, inner edge free							
0.2	15.8	10.9	0	10.9	14.6	0	14.6
0.4	15.8	10.9	0	10.9	16.3	0	16.5
0.6	20.6	18.5	0	18.5	25.9	0	25.9
0.8	38.6	65.2	0	65.2	77.6	0	77.6

Table 4. Case A, plastic buckling

γ	b/h	p	m	ρ	p^0
		Both edges clamped			
0.2	50	0.505	2	0.211	0.644
	40	0.742	2	0.462	–
0.4	60	0.545	4	0.590	–
	50	0.585	5	0.734	–
0.6	80	0.389	9	0.818	–
	75	0.395	9	0.862	–
0.8	200	0.188	20	0.841	–
	160	0.198	21	0.921	–
		Outer edge clamped, inner edge free			
0.2	25	0.642	2	0.304	–
	20	0.735	2	0.444	–
0.4	25	0.491	2	0.485	–
	20	0.605	3	0.918	–
0.6	40	0.334	3	0.638	–
	30	0.387	5	0.806	–
0.8	70	0.187	9	0.835	–
	60	0.193	12	0.879	–

Table 5. Case B, plastic buckling

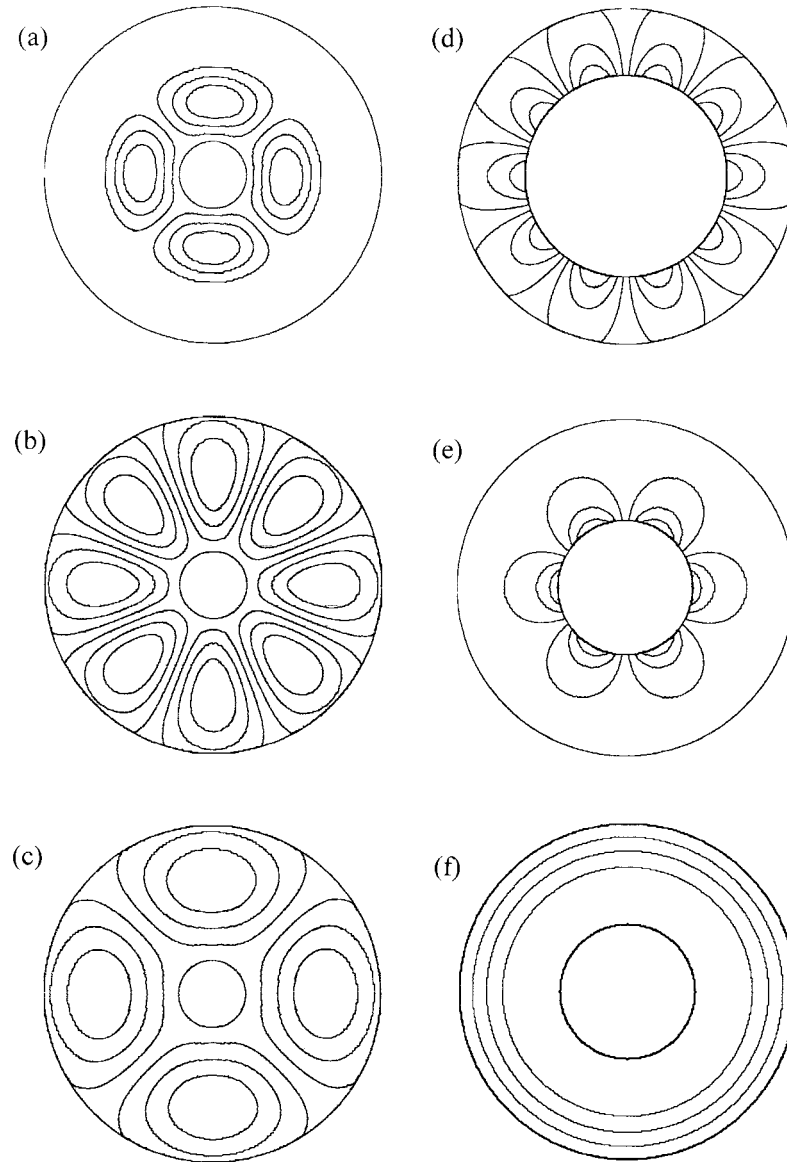| γ	b/h	p	m	ρ	p^0
		Both edges clamped			
0.2	160	0.651	4	0.226	–
	120	1.043	4	0.300	–
0.4	120	0.607	6	0.465	–
	100	0.836	6	0.564	–
0.6	140	0.399	10	0.648	–
	120	0.565	11	0.774	–
0.8	220	0.230	22	0.856	–
	210	0.276	23	0.921	–
		Outer edge clamped, inner edge free			
0.2	130	0.964	1	0.284	1.175
	110	1.155	1	0.326	1.383
0.4	90	0.687	3	0.497	1.065
	80	0.787	3	0.541	1.145
0.6	80	0.450	6	0.682	–
	60	0.564	7	0.773	–
0.8	100	0.205	14	0.827	–
	60	0.241	20	0.871	–

Fig. 4. Contour diagrams for deflection patterns: (a) Case A: $Cl + Cl$; $\gamma = 0.2$, $b/h = 40$, $m = 2$; (b) Case B: $Cl + Cl$; $\gamma = 0.2$, $b/h = 120$, $m = 4$; (c) Case C: $Cl + Cl$; $\gamma = 0.2$, $b/h = 30$, $m = 2$; (d) Case A: $Cl + Fr$; $\gamma = 0.6$, $b/h = 30$, $m = 5$; (e) Case B: $Cl + Fr$; $\gamma = 0.4$, $b/h = 80$, $m = 3$; (f) Case C: $Cl + Fr$; $\gamma = 0.4$, $b/h = 10$, $m = 0$.

7. DISCUSSION

Analysing the numerical data given in Section 6, we can draw the following conclusions.

(i) For the cases considered in this paper non-axisymmetric buckling dominates. Axisymmetric buckling leads to the lowest critical load only in Case C: $Fr + Cl$ and also in Case A: $Fr + Cl$ if $\gamma = 0.2$ (elastic buckling). In several cases no axisymmetric buckling forms were registered at all (e.g. for plastic buckling in Cases A and B). In some cases the axisymmetric buckling form exists, but it results in very high buckling loads which have no practical meaning (see, e.g., Case B: $Cl + Cl$, elastic buckling).

(ii) The number of circumferential waves m increases with the parameter γ. This conclusion is valid both for elastic and elastic-plastic buckling.

(iii) As follows from Tables 1–5, the wave numbers for elastic and plastic buckling are practically the same if both edges of the plate are clamped. This conclusion holds also for Case C: $Fr + Cl$. In Case A: $Fr + Cl$ and Case B: $Fr + Cl$, transition to plastic deformations causes the growth of wave numbers (especially for greater values of γ).

(iv) Taking into account plastic deformations, we can increase the critical loads considerably. For example, let us take Case B: $Cl + Cl$ for $\gamma = 0.2$. The elastic limit load is $p_+ = 0.48$, the plastic critical load for $b/h = 120$ is $p = 1.043$; consequently, $p/p_+ = 2.17$.

It is of interest to compare our numerical results with the results of other papers (of course, this can be done only in the case of elastic buckling, since we have no comparative data for plastic buckling). Yamaki [1] analysed buckling of annular plates under uniform compressive forces (our Case C). His parameter k can be calculated from the parameter P_{el}, according to the formula $k^2 = P_{el}$. For Case C: $Cl + Cl$, where $\gamma = 0.4$, we find $k = 10.05$ (Yamaki's value is 10.10); for Case C: $Fr + Cl$, by taking $\gamma = 0.6$, we get $k = 4.30$ (Yamaki's value is 4.29). In all cases also the wave numbers for our results and for the paper [1] strictly coincide. So, the accordance with Yamaki's results is rather good.

Next we shall concentrate on the case where tensile radial stress acts at the inner edge (our Case B). Mansfield [2] used the stress field

$$\sigma_{rM} = -\sigma_{\theta M} = p\left(\frac{\gamma}{r}\right)^2, \tag{47}$$

which is different from our Eq. (5). For this reason, along the outer edge $r = 1$ acts the stress

$$\sigma_{rM} = -\sigma_{\theta M} = p\gamma^2.$$

If we compare the circumferential stresses according to Eqs. (5) and (47), we find

$$\frac{\sigma_\theta}{\sigma_{\theta M}} = \frac{1}{1 - \gamma^2}(1 + r^2). \tag{48}$$

Since $|\sigma_\theta| > |\sigma_{\theta M}|$ and the non-axisymmetric buckling is caused mainly by the hoop stresses, Mansfield's critical loads could be expected to be greater than ours. The calculations confirm this fact. As an example let us consider Case B: $Cl + Cl$ for $\gamma = 0.1$, where $P = 1613.1$. Mansfield's loading parameter is

$$\beta_+ = \frac{\beta}{\mu}(\mu - 1)^2 = P\gamma(1 - \gamma)^2.$$

It follows from here that $\beta_+ = 131$. According to Fig. 4 in the paper [2] we have ~ 175. If $\gamma = 0.2$, we obtain $\beta_+ = 89$, while Mansfield's value is ~ 140. In both cases the wave numbers coincide with our wave numbers. Thus, in our opinion, the coincidence with Mansfield's results may be regarded as satisfactory.

8. CONCLUSIONS

A method for the investigation of the buckling of elastic-plastic annular plates was proposed. The loading and boundary conditions were chosen such that non-axisymmetric buckling could be expected. The numerical examples show that in most cases the lowest critical load is realized for non-axisymmetric buckling. The recommended method of solution is applicable also to other loading and boundary conditions which were not considered in the present paper.

ACKNOWLEDGEMENT

REFERENCES

1. Yamaki, N. Buckling of a thin annular plate under uniform compression. *J. Appl. Mech.*, 1958, **25**, 267–273.
2. Mansfield, E. H. On the buckling of an annular plate. *Quart. J. Mech. Appl. Math.*, 1960, **13**, 16–23.
3. Radwańska, M. and Waszczyszyn, Z. Numerical analysis of nonsymmetric postbuckling behaviour of elastic annular plates. *Comput. Methods Appl. Mech. Eng.*, 1980, **23**, 341–353.
4. Kumelj, T. and Kosel, F. Elastic stability of thin annular plates made of rectilinearly orthotropic material. *Comput. Struct.*, 1995, **54**, 141–145.
5. Kosel, F. and Chen Jin. Buckling of a thin annular plate subjected to two opposite locally acting pressures and supported at two opposite points. *Int. J. Mech. Sci.*, 1997, **39**, 1325–1343.
6. Laura, P. A. A., Gutiérrez, R. H., Sanzi, H. C. and Elvira, G. Buckling of circular solid and annular plates with an intermediate circular support. *Ocean Eng.*, 2000, **27**, 749–755.
7. Lepik, Ü. Optimal location of a circular support for non-axisymmetric buckling of annular plates. *Struct. Optim.*, 2002 (in print).

8. Fan, X. and Lippmann, H. Elastisch-plastisches Plattenbeulung unter thermisch erzeugten Eigenspannungen. *Z. angew. Math. Mech.*, 1997, **77**, S87–S88.

9. Timoshenko, S. *Strength of Materials, Part II*. D. Van Nostrand Co, Princeton, New Jersey, 1956.

10. Il'yushin, A. A. *Plasticity*. Goztekhizdat, 1948 (in Russian).

11. Sathyamoorthy, M. *Nonlinear Analysis of Structures*. CRC Press, New York, 1997.

12. Lepik, Ü. Axisymmetric vibrations of elastic-plastic cylindrical shells by Galerkin's method. *Int. J. Impact Eng.*, 1996, **18**, 489–504.

13. Lepik, Ü. On dynamic buckling of elastic-plastic beams. *Int. J. Non-Linear Mech.*, 2000, **35**, 721–734.

14. Lepik, Ü. Bifurcation analysis of elastic-plastic cylindrical shells. *Int. J. Non-Linear Mech.*, 1999, **34**, 299–311.

Elastsete-plastsete rõngasplaatide mittesümmeetriline stabiilsuse kadu

Ülo Lepik

On uuritud elastsete-plastsete rõngasplaatide stabiilsust rajajoontel rakendatud radiaalsete jõudude mõju korral. On eeldatud, et plaadi materjal on lineaarselt kalestuv ning allub Tresca voolavustingimusele.